ISSN: 2579-5821 (Print)
ISSN: 2579-5546 (Online)
URL address: http://journal.unhas.ac.id/index.php/geocelebes
DOI: 10.70561/geocelebes.v9i2.45404

Jurnal Geocelebes Vol. 9 No. 2, October 2025, 171 – 188

Assessment of Ground Deformation and Landslide Susceptibility Using InSAR and Hypsometric Data in Jayapura City, Papua

Nur Ayu Anas[1,5*], Harsan Ingot Hasudungan[2], Rahmat Indrajati[1,5], Marcelino N. Yonas[3,5], Harnanti Y. Hutami[4]

[1]Geological Engineering Study Program, Faculty of Engineering, Cenderawasih University, Jayapura, Papua, 99351, Indonesia.
[2]Civil Engineering Study Program, Faculty of Engineering, Cenderawasih University, Jayapura, Papua, 99351, Indonesia.
[3]Mineral Engineering Study Program, Faculty of Engineering, Cenderawasih University, Jayapura, Papua, 99351, Indonesia.
[4]Geophysical Engineering Department, Faculty of Industry and Technology, Institut Teknologi Sumatera, Lampung, 35365, Indonesia.
[5]Papua Regional Chapter of the Indonesian Association of Geologists (IAGI), Jayapura, Papua, 99351, Indonesia.

*Corresponding author. Email: ayuanas741@gmail.com

Manuscript received: 5 July 2025; Received in revised form: 18 September 2025; Accepted: 4 October 2025

Abstract

Ground deformation and landslides are major geohazards affecting Jayapura City, Papua, due to its active tectonic setting and steep topography. This study aims to assess the correlation between surface deformation and landslide susceptibility using a combination of Interferometric Synthetic Aperture Radar (InSAR) and hypsometric analysis. Sentinel-1A SAR data from ascending and descending tracks, combined with DEMNAS elevation data, were used to detect deformation patterns and evaluate geomorphological maturity through hypsometric parameters. The results reveal significant deformation patterns, including subsidence up to –0.77 m and uplift up to +0.25 m, predominantly concentrated in sub-watersheds Sw2, Sw3, and Sw4. Hypsometric analysis indicates that most sub-watersheds are in the mature geomorphological stage (HI between 0.476 and 0.495), except Sw14, which is classified as young (HI = 0.501). Validation with the landslide inventory further confirms this correlation: 75% of documented landslides occurred in areas of high deformation, while 25% were associated with moderate deformation, and none in low or stable zones. These findings provide essential insights for disaster risk reduction, highlighting priority areas for slope stabilization, land-use management, and early warning systems.

Keywords: Deformation; Hypsometric; Landslide Susceptibility; SAR Interferometry.

Citation: Anas, N. A., Hasudungan, H. I., Indrajati, R., Yonas, M. N., & Hutami, Y. H. (2025). Assessment of Ground Deformation and Landslide Susceptibility Using InSAR and Hypsometric Data in Jayapura City, Papua. *Jurnal Geocelebes*, 9(2): 171–188, doi: 10.70561/geocelebes.v9i2.45404

Introduction

Ground deformation and landslides are critical geotechnical and environmental hazards in regions with steep topography, high rainfall, and active tectonic processes. Jayapura City (Figure 1), one of the major urban centers in Papua, is located within a complex morphological zone featuring significant slope gradients and unstable geological conditions (Abrauw, 2017). Several major landslide events in the past decade have caused severe impacts on infrastructure, residential areas, and public safety.

Conventional monitoring methods, such as field surveys and geological mapping, are limited in spatial coverage and frequency. The development of remote sensing, particularly Interferometric Synthetic Aperture Radar (InSAR), enables the

detection of ground deformation with high spatial and temporal resolution. The integration of InSAR and hypsometric integral (HI) provides an effective framework for assessing slope instability and tectonic activity. InSAR has been used for landslide detection and monitoring across diverse settings (Fan et al., 2024; Guvel et al., 2023; Sorkhabi et al., 2023; Mondini et al., 2019), with further applications in wide-area mapping, precursor recognition, hazard assessment, and probabilistic modeling (Ahmad et al., 2024; Cai et al., 2023; Dai et al., 2022; Gao et al., 2025; Hu et al., 2025; Strząbała et al., 2024). Additional studies highlight its role in risk reduction, multi-sensor integration, slope deformation monitoring, and high-altitude environments (Bianchini et al., 2021; Casagli et al., 2023; Dong et al., 2025; Guo & Martínez-Graña, 2024; Lin et al., 2025; Novellino et al., 2021; Piroton et al., 2020; Yao et al., 2023; Yu et al., 2024; Zhang et al., 2024). In parallel, HI has proven valuable for linking tectonic activity and landslide susceptibility through basin morphology, DEM sensitivity, and hydrological influences (Arabameri et al., 2019; Chatterjee et al., 2024; Diercks et al., 2023; Gu et al., 2021; Gururani et al., 2023; Hang et al., 2025; Kothyari et al., 2024; Li et al., 2021; Liem et al., 2016; Makrari et al., 2022; Nikoonejad et al., 2015; Ntokos, 2025; Othman et al., 2018; Patel et al., 2024; Taloor et al., 2019; Zhang et al., 2024).

Although numerous studies have successfully applied InSAR and hypsometric analysis separately to assess ground deformation, slope instability, and tectonic activity in various regions worldwide, their combined application remains underexplored. This is particularly true in tropical, tectonically active regions with complex geomorphological settings such as Jayapura City, where integrating both approaches could significantly enhance the accuracy of landslide susceptibility assessment.

Therefore, this study aims to assess ground deformation and landslide susceptibility in Jayapura City by combining InSAR and hypsometric analysis. The findings are expected to advance landslide hazard mapping methodologies and provide scientific support for disaster risk reduction and urban planning.

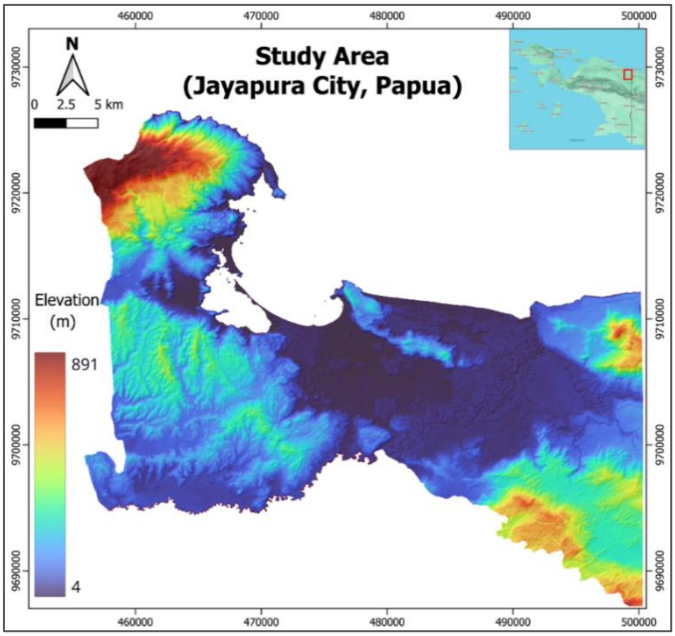

Figure 1. The study area is in Jayapura City, Papua Province, Indonesia, within the coordinate range of 460000–500000 East and 9690000–9730000 North (UTM Zone 54S). The location is presented using an elevation map to illustrate the geographical extent of the study area.

Materials and Methods

In this study, both primary and secondary datasets were utilized. The primary data consist of Sentinel-1A imagery and the Indonesian National Digital Elevation Model or DEMNAS (Badan Informasi Geospasial, 2018). The secondary data includes landslide inventory, earthquake epicenter records, and the geological map of Jayapura City. The selection of these datasets was based on their respective analytical purposes, where Sentinel-1A imagery was employed for ground deformation analysis, while DEMNAS was used for hypsometric analysis. Furthermore, the secondary data were incorporated to strengthen the spatial analysis and to validate the results obtained from the primary data processing. The specifications of the Sentinel-1A imagery used in this study are presented in Table 1.

Table 1. Sentinel-1A imagery used in this study (Alaska Satellite Facility Distributed Active Archive Center (ASF DAAC), 2025; European Space Agency, 2014).

No.	ID Scene	Acquisition	Polarization	Orbit	Abs Orbit	Spatial Resolution	Swath Width
1	S1A_IW_SLC__1SDV_20240128T085635_20240128T085701_052304_0652F0_F557	28 January 2024	VV+VH	Ascending	52304	5 x 20 m	250 km
2	S1A_IW_SLC__1SDV_20240714T085634_20240714T085700_054754_06AAC1_B8A5	14 July 2024	VV+VH	Ascending	54754	5 x 20 m	250 km
3	S1A_IW_SLC__1SDV_20250111T202114_20250111T202143_057401_0710D8_51CC	11 January 2025	VV+VH	Descending	57401	5 x 20 m	250 km
4	S1A_IW_SLC__1SDV_20250417T202112_20250417T202142_058801_07491E_079F	17 April 2025	VV+VH	Descending	58801	5 x 20 m	250 km

The InSAR processing was carried out using the SNAP 9.0 software package provided by the European Space Agency, with SNAPHU applied for phase unwrapping. Interferograms were generated from Sentinel-1A SAR data using a coherence threshold of 0.3, ensuring reliable phase stability in both vegetated and urbanized areas. For topographic phase removal and hypsometric analysis, the DEMNAS with a spatial resolution of 8.1 m was employed. A sensitivity check was also conducted by resampling DEMNAS to 15 m, which indicated no significant changes in the hypsometric integral values, thereby confirming the robustness of the results.

The selection of Sentinel-1 imagery from 2024 and 2025 was based on the need to capture the most recent ground deformation conditions in Jayapura City. Utilizing this recent temporal range allows researchers to monitor geological dynamics in real-time or near real-time, particularly concerning tectonic activity and geotechnical hazards such as landslides and land subsidence. The period from 2024 to 2025 was specifically chosen to capture ongoing change trends, ensuring that the analysis results are highly relevant to current field conditions. Moreover, this timeframe encompasses critical phases that are likely to reflect environmental responses to increased

seismic activity and geological stress in the region.

In this study, the InSAR and hypsometric methods were applied as effective tools for analyzing landslide susceptibility, particularly in tectonically active regions like Jayapura, Papua. The workflow of the applied methodology is illustrated in Figure 2.

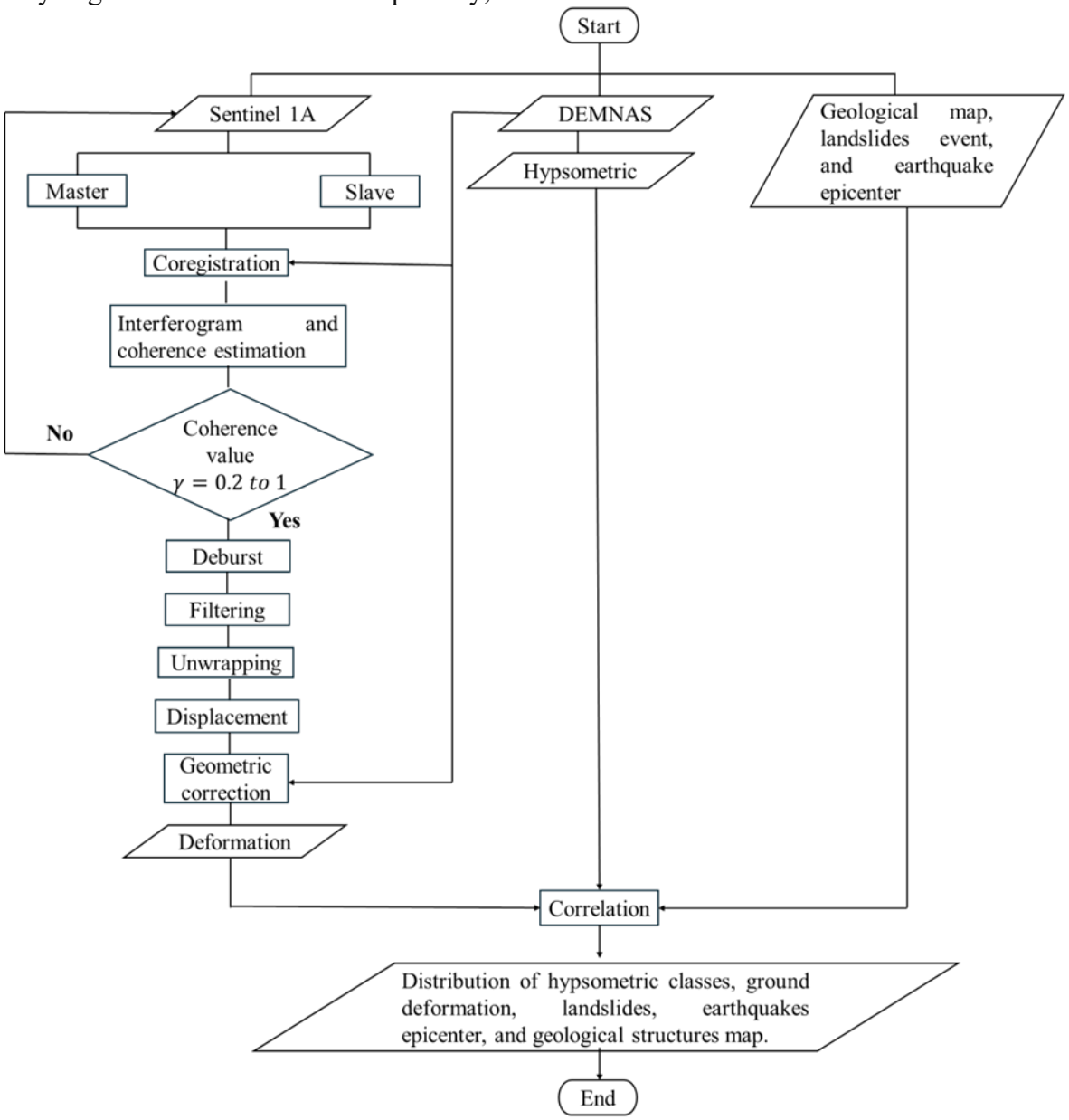

Figure 2. Research flowchart.

The Figure 2 illustrates the workflow for obtaining ground deformation values using the InSAR method. InSAR enables accurate measurements of surface deformation over large spatial scales by comparing the phase differences of radar signals acquired from two separate observations (Brengman & Barnhart, 2021; Saepuloh, 2021; Shan et al., 2024).

$$\Delta d = \frac{\lambda}{4\pi} \times \Delta\varphi \quad (1)$$

where:

Δd : surface deformation along the Line of Sight (LOS) direction (in meters)

λ : radar wavelength (for Sentinel-1A C-band, $\lambda \approx 5.6$ cm or 0.056 meters)

$\Delta\varphi$: interferometric phase difference (in radians)

4π : conversion factor from phase to displacement.

Equation (1) expresses how surface deformation along the radar line of sight (LOS) is derived from the interferometric phase difference. The displacement d is directly proportional to the phase change $\Delta\varphi$, which results from comparing two SAR acquisitions over the same area at different times. Because the radar phase is cyclic between 0 and 2π, and one full cycle corresponds to half of the radar wavelength (λ/2), the conversion factor 4π appears in the denominator. Thus, a larger phase shift indicates a larger surface displacement, while the radar wavelength λ controls the sensitivity of the measurement shorter wavelengths allow the detection of smaller ground movements.

Then the hypsometric method refers to the measurement of elevation distribution within a given area, allowing researchers to evaluate the morphology and geological development that may contribute to slope stability. This approach aligns with previous studies conducted by Aristizábal & Korup (2025). As illustrated in Figure 3, hypsometric integral (HI) values equal to or greater than 0.5 are characterized by convex-shaped curves, representing the young stage, which reflects a high level of tectonic activity. Meanwhile, HI values ranging from 0.4 to less than 0.5 indicate the intermediate (mature) stage, typically represented by straight curves or a slight combination of convex and concave forms, suggesting that tectonic activity is still present but at a moderate level. In contrast, HI values below 0.4 are associated with concave-shaped curves, corresponding to the old stage, which indicates relatively inactive tectonic conditions (Khattab et al., 2023; Liem et al., 2016; Mulyasari et al., 2017; Rabii et al., 2017).

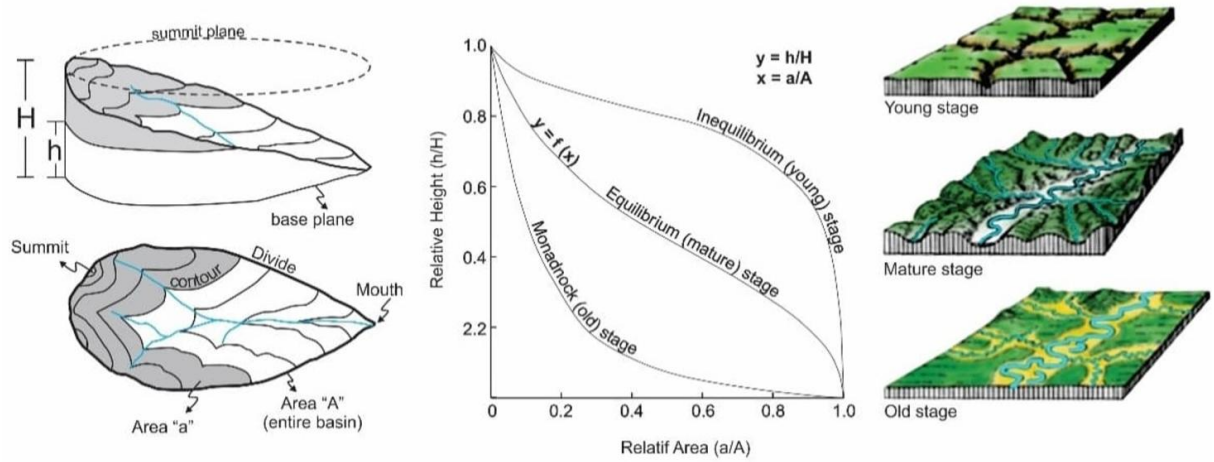

Figure 3. Schematic illustration of hypsometric analysis parameters and geomorphological stages.

In Figure 3, the schematic of hypsometric analysis parameters for a watershed (left) illustrates the relationship between relative elevation (h/H) and relative area (a/A). The hypsometric curve diagram (center), based on the concepts of (Keller & Pinter, 2002) depicts three primary patterns associated with geomorphological development stages: (1) a convex curve indicates a young stage with minimal erosion; (2) a nearly straight or slightly concave-convex curve represents the mature stage, reflecting more balanced erosion processes; and (3) a concave curve corresponds to the old stage, indicating a landscape that has been significantly worn down by long-term erosion. The right side presents illustrations of geomorphological conditions associated with each developmental stage.

The hypsometric curve is expressed in terms of the hypsometric integral (HI), which quantifies the area beneath the curve as a measure of the proportion of the basin volume that remains uneroded (Schumm, 1956). The calculation of HI follows the formula introduced by (Romero, 2024):

$$HI = \frac{\bar{h} - h_{min}}{h_{max} - h_{min}} \quad (2)$$

where:

HI : hypsometric integral

$\bar{h}$: represents the mean elevation of the geomorphic unit

h_{min} : the minimum elevation within the studied area

h_{max} : the maximum elevation within the studied area

When combined, the InSAR and hypsometric methods not only provide a comprehensive understanding of the geological and topographical conditions of the area but also enable early detection and effective management of landslide risks.

Results and Discussion

The results of this study consist of surface deformation values and hypsometric data. The surface deformation values were obtained using Sentinel-1A imagery from both ascending and descending tracks, with different acquisition time pairs as shown in Figure 4. The processed interferograms and deformation maps were utilized to detect ground movements occurring throughout the Jayapura City area, which was divided into 16 sub-watersheds (Sw1 to Sw16). This subdivision aims to facilitate spatial analysis of the deformation distribution patterns.

The results indicate that surface deformation in Jayapura City, identified through InSAR analysis using Sentinel-1A data from both ascending and descending tracks, reveals significant deformation patterns such as subsidence and uplift distributed across several sub-watersheds. Based on the ascending interferogram generated from the image pair dated January 28 to July 14, 2024, a phase change ranging from -3.12 to +3.11 radians was detected, with the densest fringe concentrations observed in Sw2, Sw3, and Sw4. The deformation map from the ascending track indicates a maximum ground subsidence of up to -0.77 m, predominantly occurring in Sw2, Sw3, and Sw4, and partially in Sw9, Sw10, Sw11, and Sw14. Meanwhile, other sub-watersheds such as Sw1, Sw5, Sw6, Sw7, Sw8, Sw12, Sw13, Sw15, and Sw16 generally show minor to insignificant deformation, indicating stable conditions.

The results from the descending track using the image pair acquired between January 11 and April 17, 2025, show a pattern consistent with that of the ascending track. The maximum uplift was recorded at +0.25 m in Sw4, with moderate uplift deformation occurring in Sw2, Sw3, Sw9, Sw10, Sw11, and Sw14, ranging from +0.072 to +0.25 m. Other areas generally exhibited insignificant deformation. The consistency of the results from both tracks strengthens the accuracy and validity of the deformation interpretation, spatially confirming that the zones with the highest deformation are concentrated in the northern part of Jayapura City, particularly within Sw2 to Sw4.

In addition to the deformation analysis, the hypsometric results (Figure 5) indicate that most sub-watersheds in Jayapura City are in the mature geomorphological stage, characterized by hypsometric integral (HI) values ranging from 0.476 to 0.495. This condition reflects that the landscape in these areas has undergone significant erosion processes while still retaining considerable relief and slope steepness. This suggests that despite prolonged erosion, slope instability potential persists due to the presence of rugged topography in several locations. Interestingly, Sw14 is the only sub-watershed classified as being in the young geomorphological stage, with a

HI value of 0.501. This indicates that Sw14 exhibits a younger morphological condition, characterized by steep topography, high relief, and a relatively low degree of erosional development compared to other sub-watersheds. However, despite its classification as geomorphologically young and the detection of localized deformation within this sub-watershed, Sw14 is not associated with fault zones or landslide occurrences during the observation period. This suggests that the instability potential in this area is primarily driven by geomorphological factors rather than tectonic activity.

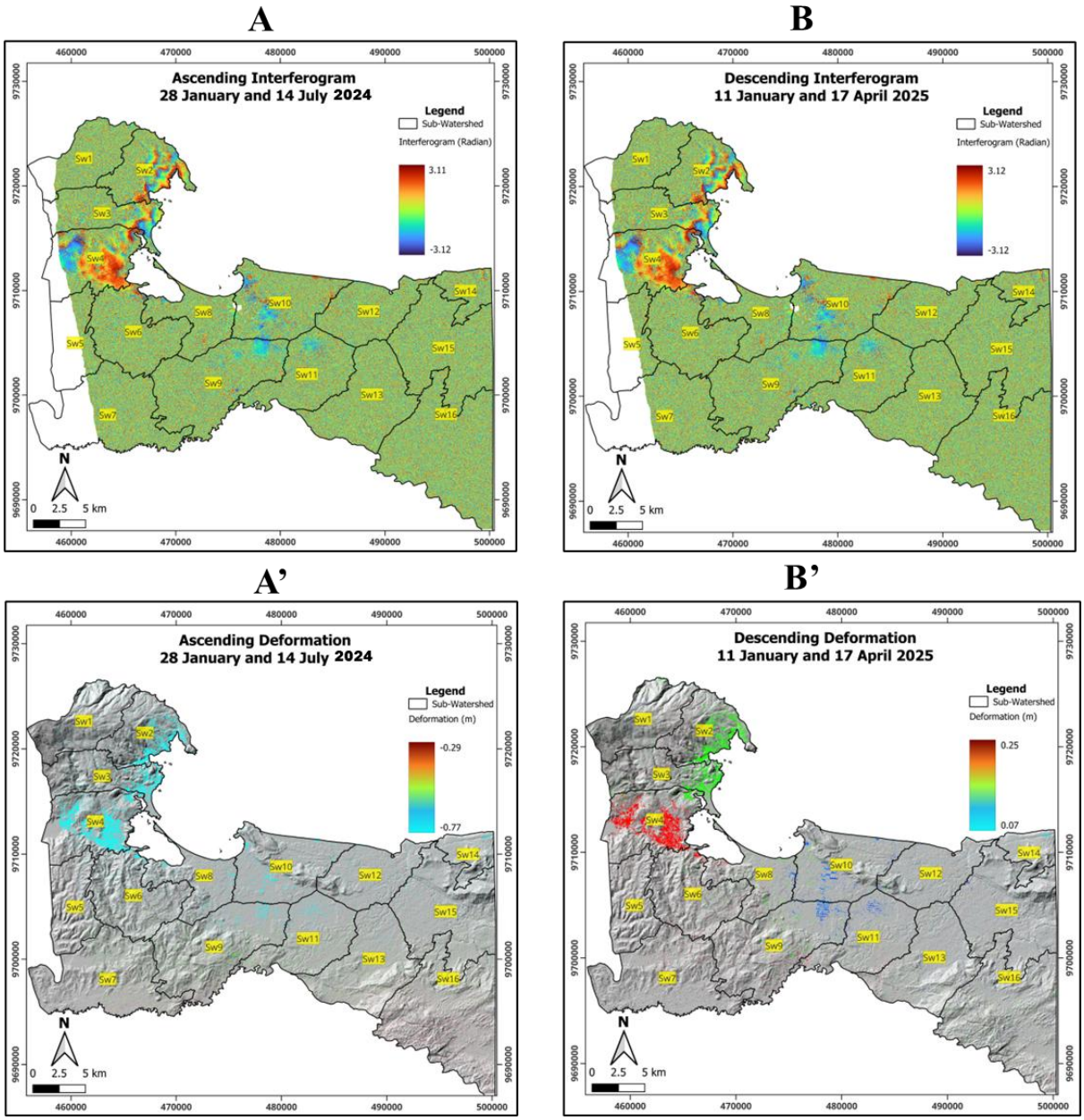

Figure 4. Surface deformation analysis in Jayapura City using Sentinel-1A SAR data: (A) interferogram from ascending pair (28 January–14 July 2024); (A′) deformation map from ascending track; (B) interferogram from descending pair (11 January–17 April 2025); (B′) deformation map from descending track.

The correlation between surface deformation, hypsometry, geological structures, earthquake epicenter distribution from 2002 to 2025, and landslide occurrences in Jayapura City reveals a strong interconnection (Figure 6). The presence of a thrust fault trending northwest–southeast (NW–SE) within the

metamorphic rocks of the Cycloops Schist Complex (pTmc), which represent a metamorphic facies zone, serves as the primary control of the deformation observed in Sw3 and Sw4. The hard but brittle nature of the metamorphic rocks in this zone acts as a medium for the accumulation and release of compressive stress, which actively triggers vertical deformation. In addition to thrust faulting, patterns of lateral deformation and uplift are also controlled by normal faults dominantly trending north-northwest–south-southeast (NNW–SSE) and west-southwest–east-northeast (WSW–ENE), as well as strike-slip faults trending WSW–ENE, which are distributed across several sub-watersheds, particularly from Sw2 to Sw9 and Sw12. The occurrence of faults along the boundary between the Ultramafic Rock Formation (Um), composed of harzburgite, serpentinite, pyroxenite, and dunite, and the Nubai Formation (Tomn), dominated by limestone interbedded with biomicrite, marl, fine-grained sandstone, and tuffaceous greywacke, further emphasizes the structural complexity of Jayapura, where strong lithological contrasts promote deformation concentration (Welikanna & Jin, 2023).

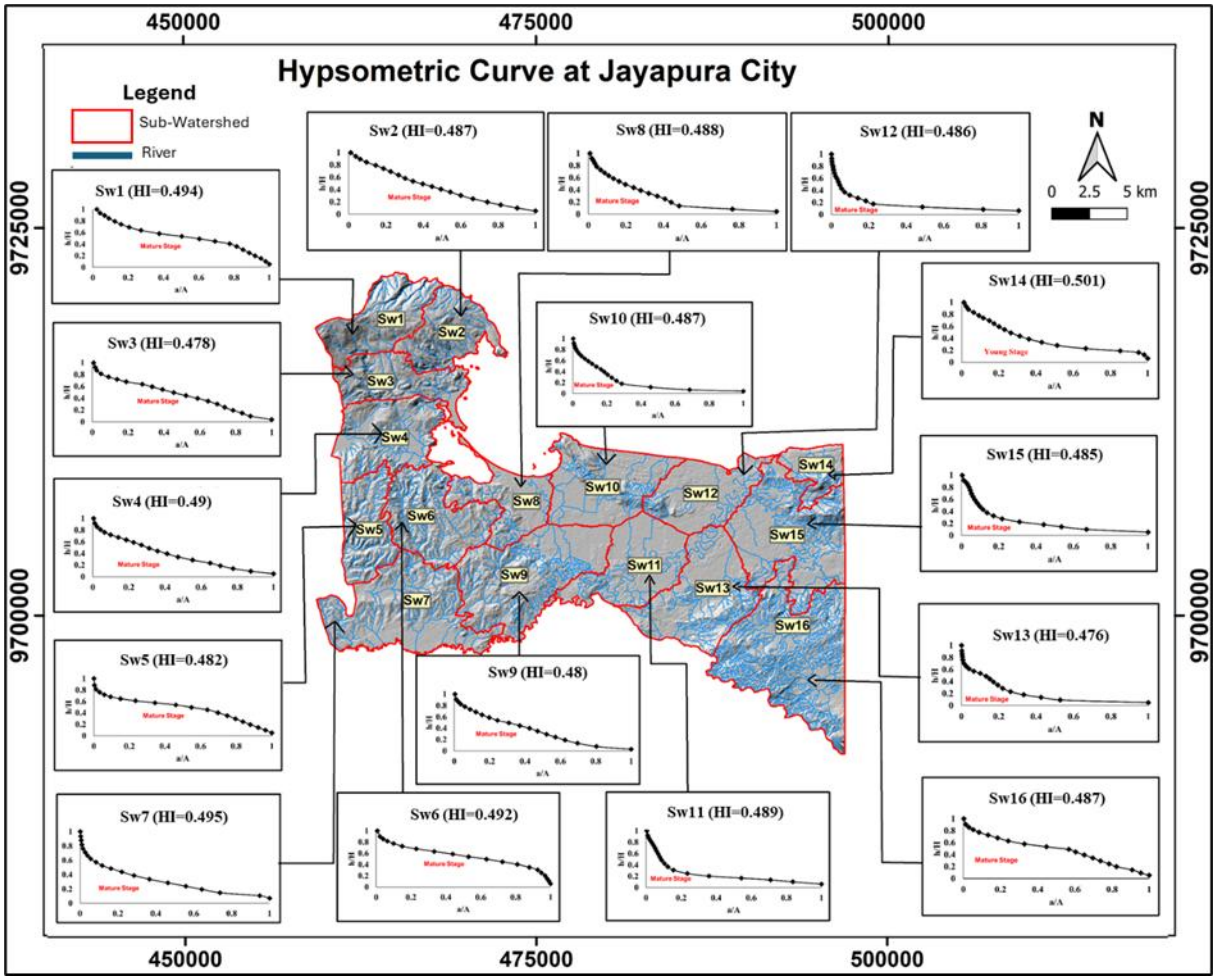

Figure 5. Hypsometric curves of 16 sub-watersheds (Sub-DAS) in Jayapura City. The hypsometric integral (HI) values are used to assess the geomorphological development stage of each sub-watershed.

This tectonic complexity does not act in isolation but interacts strongly with the lithological framework of Jayapura. The convergence of multiple weak sedimentary formations further amplifies the impact of fault activity, making the area more prone to both vertical and lateral deformation. The Makats Formation (Tmm) consists of greywacke, siltstone, shale, marl, conglomerate, interbedded limestone, tuff,

and volcanic breccia. Meanwhile, the Jayapura Formation (Qpj) comprises coral-algal limestone, calcirudite, calcarenite, marl, and reef-structured limestone (Suwarna & Noya, 1995). The combination of lithologies from the Makats, Nubai, and Jayapura Formations, which are dominated by weak sedimentary rocks with low cohesion, makes the area highly susceptible to both vertical (subsidence and uplift) and lateral deformation. This inherent lithological weakness, when combined with active fault movements, leads to significant stress accumulation and deformation across multiple sub-watersheds.

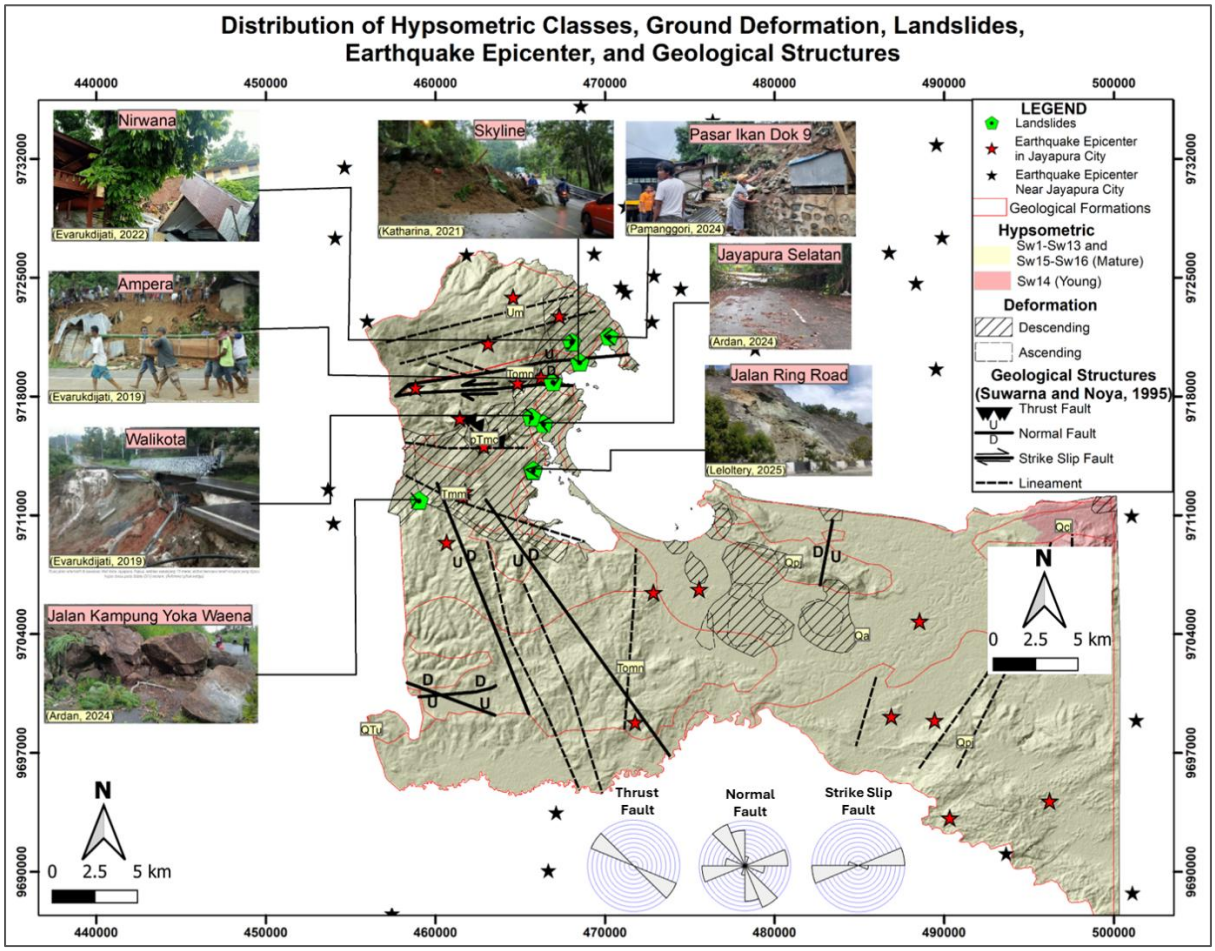

Figure 6. Distribution of deformation, hypsometry, landslides, earthquake epicenters, geological structures, and lithological formations in Jayapura City.

In addition, the spatial distribution of earthquake epicenters from 2002 to 2025 shows a proximity to several documented landslide locations, particularly in Sw2, Sw3, and Sw4 (Figure 6). This spatial relationship suggests that seismic activity may act as a triggering factor that accelerates slope failure in areas already weakened by active deformation and fragile lithologies. The potential activity of these faults leads to stress accumulation that promotes deformation in soils and rocks with inherently weak mechanical properties. InSAR effectively captures deformation in these areas due to a combination of fault block movements, the presence of fractures or shear zones, and the reduction in rock strength caused by weathering or subsurface moisture changes (Alonso-Díaz et al., 2023; Farolfi et al., 2019). In addition to tectonic factors, the presence of lithologies such as marl, shale, and conglomerate—materials that are highly compressible and plastically deformable (Staniewicz & Chen, 2024) further amplifies the surface deformation

response, which is clearly recorded in the InSAR results. Conversely, the deformation detected in Sw10 and Sw11, which are underlain by the Qa Formation consisting of alluvium and coastal deposits, is unrelated to tectonic activity. Instead, it is attributed to non-tectonic factors, particularly rapid land-use changes associated with intensive urban development, which appear as deformation signals in the InSAR analysis.

Table 2 . Deformation classification and landslide occurrences in sub-watersheds of Jayapura city.

No.	Sub-watershed	Sub-watershed Area (ha)	Deformation Area (ha)	Percentage of Deformation Area (%)	Deformation Classification	Total landslide Events 2019-2025	Location
1	Sw1	4149.23	-	-	No deformation	-	-
2	Sw2	3628.46	2317.19	63.86	High	4	Kawasan Ampera, Nirwana, Pasar Ikan Dok 9, and Skyline
3	Sw3	3643.76	1459.32	40.05	Moderate	2	Kantor Distrik Jayapura Selatan and Kantor Walikota
4	Sw4	4897	4128.59	84.31	High	2	Kampung Yoka Waena and Jalan Ringroad
5	Sw5	3482.58	7.67	0.22	No deformation	-	-
6	Sw6	5307.22	438.88	8.27	Low	-	-
7	Sw7	7671.4	-	-	No deformation	-	-
8	Sw8	3431.34	280.38	8.17	Low	-	-
9	Sw9	7738.04	930.15	12.02	Low	-	-
10	Sw10	5597.85	1551.6	27.72	Moderate	-	-
11	Sw11	4995.9	899.73	18.01	Low	-	-
12	Sw12	4255.3	84.02	1.97	Low	-	-
13	Sw13	6323.65	-	-	No deformation	-	-
14	Sw14	1806.58	126.39	6.99	Low	-	-
15	Sw15	7838.1	-	-	No deformation	-	-
16	Sw16	10029.7	-	-	No deformation	-	-

Table 3. Landslide distribution by deformation class.

Deformation Classification	Landslide Events	Percentage (%)
High	6	75.0
Moderate	2	25.0
Low	0	0.0
No deformation	0	0.0

The occurrence of landslides along several locations, including Jalan Kampung Yoka Waena, the area surrounding the Walikota's Office, Ampera, Nirwana, Jalan Skyline, Pasar Ikan Dok 9, Jayapura Selatan, and Jalan Ringroad (Ardan, 2024; Evarukdijati, 2019a, 2019b, 2022; Katharina, 2021; Leloltery, 2025; Pamanggori, 2024), further supports the observation that landslide events are predominantly concentrated in areas experiencing a combination of active deformation and mature hypsometric conditions, particularly in Sw2, Sw3, and Sw4. To strengthen this correlation, a quantitative validation was conducted by comparing deformation zones with the landslide inventory from 2019 – 2025. For this purpose, it is developed our own deformation classification system based on

the proportion of affected area within each sub-watershed, which are: No deformation (0%), Low deformation (1–25%), Moderate deformation (26–50%), and High deformation (51–100%).

The results are summarized in Table 2 and Table 3, which demonstrates that sub-watersheds Sw2, Sw3, and Sw4, categorized as high to moderate deformation zones (40–84% coverage), correspond with many documented landslide events. In contrast, areas with low or no deformation show either minor or no landslide occurrences. This quantitative validation is consistent with the geological and geomorphological evidence, as ongoing deformation in these areas likely increases slope stress and instability.

In these areas, ongoing deformation likely increases slope stress, which is further exacerbated by the presence of weak lithologies such as marl, clay, brecciated ultramafic rocks, and weathered serpentinite. These conditions render the slopes highly unstable and susceptible to landslides, especially when triggered by extreme rainfall or seismic activity. Conversely, although Sw14 exhibits steep morphology, a high HI value, and detectable deformation, no landslide events have been identified in this area. This indicates that the hazard potential in Sw14 is more latent and primarily associated with long-term geomorphological processes rather than active tectonic deformation.

In order to strengthen the interpretation, landslide events recorded between 2019 and 2025 were analyzed in relation to the deformation classification. The number of landslide events was compared across different deformation classes, as summarized in Table 3.

Validation of the deformation zones using the landslide inventory data indicates a strong spatial correlation. Out of a total of eight recorded landslide events, six events (75%) occurred within areas classified as High deformation, while two events (25%) were in the Moderate deformation zones. No landslides were observed in areas categorized as Low deformation or No deformation. These results demonstrate that the deformation zones mapped from InSAR analysis correspond well with the actual landslide occurrences, particularly within the high deformation areas.

This consistency is in line with previous studies support the findings of this research by emphasizing the strong relationship between ground deformation and landslide susceptibility. Miao et al., (2023) and Wu et al., (2024) highlighted that areas experiencing significant deformation are more prone to slope failures, and that incorporating InSAR data substantially improves landslide risk evaluation. Dai et al., (2022), Lau et al., (2024), and Ran et al., (2023) further demonstrated that advanced InSAR techniques such as SBAS and PS-InSAR are highly effective in detecting subtle ground movements, particularly in mountainous terrains. In addition, hypsometric analysis has been widely used to link geomorphic evolution with landslide potential, where youthful basins with higher hypsometric integral values tend to show greater instability (Vijith et al., 2017). The integration of InSAR-derived deformation with hypsometric parameters has therefore been recognized as a robust framework for improving landslide susceptibility assessments (Gera & Agegnehu, 2021; Ramzan et al., 2022).

Overall, this study highlights that landslide susceptibility in Jayapura City is governed by the interaction of two main factors: ongoing tectonic activity, particularly along thrust, normal, and strike-slip fault zones in Sw2, Sw3, and Sw4; and non-tectonic factors such as extensive land-use changes (Juna, 2025), especially in Sw10 and Sw11. These findings have significant implications for urban planning and disaster mitigation strategies in Jayapura

City. Areas characterized by active uplift, subsidence, mature hypsometric conditions, and weak lithologies should be prioritized in mitigation programs, including slope reinforcement, land-use regulation, and the implementation of early warning systems. Additionally, although areas like Sw14 currently show no recorded landslides, they should remain under close observation due to their steep geomorphological characteristics and latent instability potential, which may be exacerbated by ongoing denudation processes and increased human activities in the future.

Despite the comprehensive spatial analysis presented in this study, there are several limitations that should be acknowledged. The assessment relies solely on InSAR-derived deformation and hypsometric data, without incorporating other critical factors such as soil mechanical properties, rainfall intensity, and subsurface conditions. Therefore, the deformation patterns and slope instability identified represent preliminary indicators based on geomorphological and tectonic parameters rather than a complete landslide hazard assessment.

Conclusion

This study demonstrates that landslide susceptibility in Jayapura City is primarily governed by the interaction between tectonic deformation and geomorphological factors. InSAR analysis reveals significant uplift and subsidence concentrated in sub-watersheds Sw2, Sw3, and Sw4, which also correspond to areas with documented landslide events. The hypsometric assessment further highlights the role of mature to old geomorphic stages in amplifying slope instability. The integration of InSAR-derived deformation and hypsometric parameters thus provides an effective framework for identifying high-risk zones, with practical implications for slope reinforcement, land-use planning, and the development of early warning systems to reduce disaster risk in Jayapura City.

Despite these findings, several limitations should be acknowledged. The accuracy of InSAR analysis is influenced by atmospheric noise, temporal and spatial decorrelation, and the resolution of DEM data used for phase removal. Moreover, the study did not incorporate other key factors such as rainfall intensity, soil mechanical properties, and groundwater conditions, which are critical for comprehensive landslide hazard assessment. Therefore, the results should be considered preliminary indicators of slope instability. Future research combining multi-sensor SAR time-series, hydrological records, and geotechnical field validation will be essential to refine hazard mapping and support more robust disaster mitigation strategies in Jayapura City.

Acknowledgements

The authors gratefully acknowledge the Lembaga Penelitian dan Pengabdian kepada Masyarakat (LPPM) Universitas Cenderawasih for providing financial support for this research.

Author Contribution

All authors contributed substantially to this research. NAA contributed to the conceptualization, methodology, and writing original draft. HIH was responsible for investigation (landslide analysis) and visualization. RI and MNY conducted structural and tectonic analysis. HYH was responsible for integration of datasets. All authors contributed to writing, review, editing, and approved the final manuscript.

Conflict of Interest

The authors declare that there are no known financial or personal conflicts of interest

that could have appeared to influence the work reported in this paper.

References

Abrauw, R. D. (2017). Wilayah rawan longsor di Kota Jayapura. *Jurnal Geografi Lingkungan Tropik*, 1(1), 2. https://doi.org/10.7454/jglitrop.v1i1.4

Ahmad, M. S., Lisa, M., & Khan, S. (2024). Assessment and mapping of landslides in steep mountainous terrain using PS-InSAR: A case study of Karimabad Valley in Chitral. *Kuwait Journal of Science*, 51(1), 100137. https://doi.org/10.1016/j.kjs.2023.09.007

Alaska Satellite Facility Distributed Active Archive Center (ASF DAAC). (2025). *Sentinel-1 data search and download portal*. University of Alaska Fairbanks. https://search.asf.alaska.edu/

Alonso-Díaz, A., Casado-Rabasco, J., Solla, M., & Lagüela, S. (2023). Using InSAR and GPR Techniques to Detect Subsidence: Application to the Coastal Area of "A Xunqueira" (NW Spain). *Remote Sensing*, 15(15), 3729. https://doi.org/10.3390/rs15153729

Arabameri, A., Pradhan, B., Rezaei, K., & Lee, C.-W. (2019). Assessment of landslide susceptibility using statistical- and artificial intelligence-based FR-RF integrated model and multiresolution DEMs. *Remote Sensing*, 11(9), 999. https://doi.org/10.3390/rs11090999

Ardan. (2024). *Jayapura Hujan Deras, Akibatkan Longsor dan Banjir*. Radio Republik Indonesia Jayapura (RRI). https://www.rri.co.id/daerah/1199068/jayapura-hujan-deras-akibatkan-longsor-dan-banjir

Aristizábal, E., & Korup, O. (2025). Linking Landslide Patterns to Transient Landscapes in the Northern Colombian Andes. *Journal of Geophysical Research: Earth Surface*, 130(3), e2024JF008027. https://doi.org/10.1029/2024JF008027

Badan Informasi Geospasial. (2018). *DEMNAS*. Bada Informasi Geospasial. https://tanahair.indonesia.go.id/portal-web/unduh/demnas

Bianchini, S., Solari, L., Bertolo, D., Thuegaz, P., & Catani, F. (2021). Integration of satellite interferometric data in civil protection strategies for landslide studies at a regional scale. *Remote Sensing*, 13(10), 1881. https://doi.org/10.3390/rs13101881

Brengman, C. M. J., & Barnhart, W. D. (2021). Identification of Surface Deformation in InSAR Using Machine Learning. *Geochemistry, Geophysics, Geosystems*, 22(3), 1–15. https://doi.org/10.1029/2020GC009204

Cai, J., Zhang, L., Dong, J., Guo, J., Wang, Y., & Liao, M. (2023). Automatic identification of active landslides over wide areas from time-series InSAR measurements using Faster RCNN. *International Journal of Applied Earth Observation and Geoinformation*, 124(November), 103516. https://doi.org/10.1016/j.jag.2023.103516

Casagli, N., Intrieri, E., Tofani, V., Gigli, G., & Raspini, F. (2023). Landslide detection, monitoring and prediction with remote-sensing techniques. *Nature Reviews Earth and Environment*, 4(1), 51–64. https://doi.org/10.1038/s43017-022-00373-x

Chatterjee, S., Ansari, K., Biswas, M., Mukherjee, S., & Kavitha, B. (2024). Morphometry and active tectonics of the Konkan coast, western India. *Evolving Earth*, 2(January), 100041. https://doi.org/10.1016/j.eve.2024.100041

Dai, K., Deng, J., Xu, Q., Li, Z., Shi, X., Hancock, C., Wen, N., Zhang, L., & Zhuo, G. (2022). Interpretation and

sensitivity analysis of the InSAR line of sight displacements in landslide measurements. *GIScience and Remote Sensing*, 59(1), 1226–1242. https://doi.org/10.1080/15481603.2022.2100054

Diercks, M.-L., Grützner, C., Welte, J., & Ustaszewski, K. (2023). Challenges of geomorphologic analysis of active tectonics in a slowly deforming karst landscape (W Slovenia and NE Italy). *Geomorphology*, 440(November), 108894. https://doi.org/10.1016/j.geomorph.2023.108894

Dong, J., Guo, Y., Mei, Y., & Gao, K. (2025). Deformation monitoring and safety stability evaluation study of high-altitude limestone dumps. *PLoS ONE*, 20(2 February), 1–27. https://doi.org/10.1371/journal.pone.0318589

European Space Agency. (2014). *Sentinel-1 SAR data*. Copernicus Open Access Hub. https://sentinels.copernicus.eu/web/sentinel/missions/sentinel-1

Evarukdijati. (2019a). *Banjir dan Tanah Longsor melanda kota jayapura*. Antara News. https://papua.antaranews.com/berita/475037/banjir-dan-tanah-longsor-melanda-kota-jayapura

Evarukdijati. (2019b). *Longsor di Kawasan Ampera Kota Jayapura, empat orang meninggal*. https://www.antaranews.com/berita/811167/longsor-di-kawasan-ampera-kota-jayapura-empat-orang-meninggal

Evarukdijati. (2022). *Tanah longsor menyebabkan tujuh orang meninggal di Kota Jayapura*. Antara News.

Fan, B., Luo, G., Hellwich, O., Shi, X., Yuan, X., Ma, X., Shang, M., & Wang, Y. (2024). Monitoring Creeping Landslides with InSAR in a Loess-covered Mountainous Area in the Ili Valley, Central Asia. *PFG - Journal of Photogrammetry, Remote Sensing and Geoinformation Science*, 92(3), 235–251. https://doi.org/10.1007/s41064-024-00292-0

Farolfi, G., Del Soldato, M., Bianchini, S., & Casagli, N. (2019). A procedure to use GNSS data to calibrate satellite PSI data for the study of subsidence:an example from the north-western Adriatic coast (Italy). *European Journal of Remote Sensing*, 52(sup4), 54–63. https://doi.org/10.1080/22797254.2019.1663710

Gao, X., Wang, B., Dai, W., & Liu, Y. (2025). A landslide susceptibility assessment method using SBAS-InSAR to optimize Bayesian network. *Frontiers in Environmental Science*, 13(February), 1–25. https://doi.org/10.3389/fenvs.2025.1522949

Gera, S., & Agegnehu, N. (2021). Landslide Susceptible Mapping using InSAR and GIS Techniques: A Case Study at Debresina Area, Ethiopia. *Journal of Geology and Geophysics*, 10(3), 988. https://www.longdom.org/open-access-pdfs/landslide-susceptible-mapping-using-insar-and-gis-techniques-overview-of-debresina-area-ethiopia.pdf

Gu, Z.-K., Yao, X., Yao, C.-C., & Li, C.-G. (2021). Mapping of geomorphic dynamic parameters for analysis of landslide hazards: A case of Yangbi river basin on the upper Lancang-Mekong of China. *Journal of Mountain Science*, 18(9), 2402–2411. https://doi.org/10.1007/s11629-021-6795-2

Guo, H., & Martínez-Graña, A. M. (2024). Susceptibility of Landslide Debris Flow in Yanghe Township Based on Multi-Source Remote Sensing Information Extraction Technology (Sichuan, China). *Land*, 13(2), 206. https://doi.org/10.3390/land13020206

Gururani, K., Kothyari, G. C., & Kotlia, B.

S. (2023). Morphotectonic assessment of the Gaula river basin, Kumaun lesser Himalaya, Uttarakhand. *Quaternary Science Advances*, 12(October), 100115. https://doi.org/10.1016/j.qsa.2023.100115

Guvel, Ş. P., Akgul, M. A., & Akkoyunlu, M. F. (2023). Monitoring and Evaluation of 2015 Devrek Zonguldak Landslide within the scope of Flood Risk Assessment by Landsat-8 Satellite Data. *Doğal Afetler ve Çevre Dergisi*, 9(1), 81–89. https://doi.org/10.21324/dacd.1152670

Hang, P. T. T., Shakirov, R., Thom, B. V., Dung, L. V., Syrbu, N., Hieu, T. T., Anh, P. T. N., Yen, T. H., Maltseva, E., Kholmogorov, A., Tuyen, N. H., & An, V. H. (2025). Assessment of the Tectonic Activity of the Muong La–Bac Yen–Cho Bo Fault (Northwest Vietnam) by Analysis of Geomorphological Indices. *GeoHazards*, 6(2), 16. https://doi.org/10.3390/geohazards6020016

Hu, X., Sun, Z., Wang, Z., Huang, X., Zhou, M., He, S., Xiao, H., Liu, D., Yang, Y., & Xu, W. (2025). InSAR-based deep learning prediction model for multi-type landslides displacement and failure time in Zigui, Three Gorges Area, China. *Landslides,* (2025). https://doi.org/10.1007/s10346-025-02613-9

Juna. (2025). *900 Unit Perumahan Grand Royal Residen II akan Dibangun di Holtekamp*. Cenderawasih Pos. https://cenderawasihpos.jawapos.com/ekonomi-bisnis/04/02/2025/900-unit-perumahan-grand-royal-residen-ii-akan-dibangun-di-holtekamp/%0A

Katharina. (2021). *Jayapura Rawan Longsor, Warga Harus Waspada*. Kumparan. https://kumparan.com/bumi-papua/jayapura-rawan-longsor-warga-harus-waspada-1vE0VmMh3zo/full

Keller, E. A., & Pinter, N. (2002). Active Tectonics Earthquakes, Uplift, and Landscape. In *Prentice Hall earth science series* (second edi). Prentice Hall. https://doi.org/10.2113/gseegeosci.iii.3.463

Khattab, M. I., Abotalib, A. Z., Othman, A., & Selim, M. K. (2023). Evaluation of multiple digital elevation models for hypsometric analysis in the watersheds affected by the opening of the Red Sea. *The Egyptian Journal of Remote Sensing and Space Science*, 26(4), 1020–1035. https://doi.org/10.1016/j.ejrs.2023.11.011

Kothyari, H. C., Kothyari, G. C., Joshi, R. C., Gururani, K., Nandy, S., & Patidar, A. K. (2024). Assessment of fluvial response to landslide susceptibility and transient response of tectonically active upper Alaknanda River basin of Uttarakhand Himalaya, India. *Quaternary Science Advances*, 15(September), 100221. https://doi.org/10.1016/j.qsa.2024.100221

Lau, R., Seguí, C., Waterman, T., Chaney, N., & Veveakis, M. (2024). InSAR-informed in situ monitoring for deep-seated landslides: insights from El Forn (Andorra). *Natural Hazards and Earth System Sciences*, 24(10), 3651–3661. https://doi.org/10.5194/nhess-24-3651-2024

Leloltery, A. (2025). *BPBD Papua: Longsor Jalan Ring Road Kota Jayapura Perlu Penanganan Serius*. Antara News. https://papua.antaranews.com/berita/735782/bpbd-papua-longsor-jalan-ring-road-kota-jayapura-perlu-penanganan-serius

Li, C., Yi, B., Gao, P., Li, H., Sun, J., Chen, X., & Zhong, C. (2021). Valuable clues for dcnn-based landslide detection from a comparative

assessment in the wenchuan earthquake area. *Sensors*, 21(15), 5191. https://doi.org/10.3390/s21155191

Liem, N. V., Dat, N. P., Dieu, B. T., Phai, V. V., Trinh, P. T., Vinh, H. Q., & Phong, T. V. (2016). Assessment of Geomorphic Processes and Active Tectonics in Con Voi Mountain Range Area (Northern Vietnam) Using the Hypsometric Curve Analysis Method. *Vietnam Journal of Earth Sciences*, 38(2), 202–216. https://doi.org/10.15625/0866-7187/38/2/8602

Lin, N., Ding, K., Tan, L., Li, B., Yang, K., Wang, C., Wang, B., Li, N., & Yang, R. (2025). Dynamic landslide susceptibility mapping on time-series InSAR and explainable machine learning: a case study at Wushan in the Three Gorges Reservoir area, China. *Advances in Space Research*, 75(12), 8439–8465. https://doi.org/10.1016/j.asr.2025.03.067

Makrari, S., Sharma, G., Taloor, A. K., Singh, M. S., Sarma, K. K., & Aggarwal, S. P. (2022). Assessment of the geomorphic indices in relation to tectonics along selected sectors of Borpani River Basin, Assam using Cartosat DEM data. *Geosystems and Geoenvironment*, 1(3), 100068. https://doi.org/10.1016/j.geogeo.2022.100068

Miao, F., Ruan, Q., Wu, Y., Qian, Z., Kong, Z., & Qin, Z. (2023). Landslide Dynamic Susceptibility Mapping Base on Machine Learning and the PS-InSAR Coupling Model. *Remote Sensing*, 15(22), 5427. https://doi.org/10.3390/rs15225427

Mondini, A. C., Santangelo, M., Rocchetti, M., Rossetto, E., Manconi, A., & Monserrat, O. (2019). Sentinel-1 SAR amplitude imagery for rapid landslide detection. *Remote Sensing*, 11(7), 0760. https://doi.org/10.3390/rs11070760

Mulyasari, R., Brahmantyo, B., & Supartoyo. (2017). Morphometric analysis of relative tectonic activity in the Baturagung Mountain, Central Java, Indonesia. *IOP Conference Series: Earth and Environmental Science*, 71(1), 012006. https://doi.org/10.1088/1755-1315/71/1/012006

Nikoonejad, A., Pourkermani, M., Asadi, A., & Almasian, M. (2015). Hypsometric Properties of South Zagros Fold-Thrust Belt Basins: A Case Study in Namdan Basin in SW Iran. *Open Journal of Geology*, 5(10), 701–717. https://doi.org/10.4236/ojg.2015.510062

Novellino, A., Cesarano, M., Cappelletti, P., Di Martire, D., Di Napoli, M., Ramondini, M., Sowter, A., & Calcaterra, D. (2021). Slow-moving landslide risk assessment combining Machine Learning and InSAR techniques. *Catena*, 203(August), 105317. https://doi.org/10.1016/j.catena.2021.105317

Ntokos, D. (2025). Unveiling tectonic activity through lithological-erosional interplay with the Tectonic Processes Index Tδ. *Journal of Asian Earth Sciences*, 291(September), 106680. https://doi.org/10.1016/j.jseaes.2025.106680

Othman, A. A., Gloaguen, R., Andreani, L., & Rahnama, M. (2018). Improving landslide susceptibility mapping using morphometric features in the Mawat area, Kurdistan Region, NE Iraq: Comparison of different statistical models. *Geomorphology*, 319, 147–160. https://doi.org/10.1016/j.geomorph.2018.07.018

Pamanggori. (2024). *Longsor menimpa Pasar Ikan Dok 9 Namun Tidak Ada Korban Jiwa*. Noken Live. https://www.nokenlive.com/2024/12/18/longsor-menimpa-pasar-ikan-dok-

9-namun-tidak-ada-korban-jiwa/

Patel, D. K., Thakur, T. K., Saini, S., Patel, A., Bhatt, S. C., Kumar, A., Kumar, R., & Husain, F. M. (2024). Morphometric indices assessment: Implications for active tectonics in the upper Narmada Basin, central India. *Physics and Chemistry of the Earth*, 136(December), 103746. https://doi.org/10.1016/j.pce.2024.103746

Piroton, V., Schlögel, R., Barbier, C., & Havenith, H.-B. (2020). Monitoring the recent activity of landslides in the Mailuu-Suu valley (Kyrgyzstan) using radar and optical remote sensing techniques. *Geosciences*, 10(5), 164. https://doi.org/10.3390/geosciences10050164

Rabii, F., Achour, H., Rebai, N., & Jallouli, C. (2017). Hypsometric integral for the identification of neotectonic and lithology differences in low tectonically active area (Utica-Mateur region, north-eastern Tunisia). *Geocarto International*, 32(11), 1229–1242. https://doi.org/10.1080/10106049.2016.1195890

Ramzan, U., Fan, H., Aeman, H., Ali, M., & Al-qaness, M. A. A. (2022). Combined analysis of PS-InSAR and hypsometry integral (HI) for comparing seismic vulnerability and assessment of various regions of Pakistan. *Scientific Reports*, 12, 22423. https://doi.org/10.1038/s41598-022-26159-1

Ran, P., Li, S., Zhuo, G., Wang, X., Meng, M., Liu, L., Chen, Y., Huang, H., Ye, Y., & Lei, X. (2023). Early Identification and Influencing Factors Analysis of Active Landslides in Mountainous Areas of Southwest China Using SBAS−InSAR. *Sustainability (Switzerland)*, 15(5), 4366. https://doi.org/10.3390/su15054366

Romero, R. V. (2024). Application of Geographic Information System (GIS) for Hypsometric Analysis of a Bicol River Basin Area. *Engineering and Technology Journal*, 09(08), 4787–4794. https://doi.org/10.47191/etj/v9i08.25

Saepuloh, A. (2021). *Prinsip dan aplikasi penginderaan jauh geologi gunungapi*. ITB Press.

Schumm, S. A. (1956). Geological Society of America Bulletin Evolution Of Drainage Systems And Slopes In Badlands At Perth Amboy , New Jersey. *Bulletin of the Geological Society of America*, 67(5), 597–646. https://doi.org/10.1130/0016-7606(1956)67

Shan, Y., Xu, Z., Zhou, S., Lu, H., Yu, W., Li, Z., Cao, X., Li, P., & Li, W. (2024). Landslide Hazard Assessment Combined with InSAR Deformation: A Case Study in the Zagunao River Basin, Sichuan Province, Southwestern China. *Remote Sensing*, 16(1), 99. https://doi.org/10.3390/rs16010099

Sorkhabi, O. M., Khajehzadeh, M., & Keawsawasvong, S. (2023). Landslides monitoring with SBAS-InSAR and GNSS. *Physics and Chemistry of the Earth*, 132(December), 103486. https://doi.org/10.1016/j.pce.2023.103486

Staniewicz, S., & Chen, J. (2024). Automatic Detection of InSAR Surface Deformation Signals in the Presence of Severe Tropospheric Noise, *TechRxiv*, 1–12. https://doi.org/10.36227/techrxiv.20128406.v2

Strząbała, K., Ćwiąkała, P., & Puniach, E. (2024). Identification of Landslide Precursors for Early Warning of Hazards with Remote Sensing. *Remote Sensing*, 16(15), 2781. https://doi.org/10.3390/rs16152781

Suwarna, N., & Noya, Y. (1995). *Peta geologi lembar Jayapura (Pegunungan Cycloops), Irian Jaya*.

Pusat Penelitian dan Pengembangan Geologi (P3G). Bandung.

Vijith, H., Prasannakumar, V., & Pratheesh, P. (2017). Landform evaluation through hypsometric characterisation: An example from a selected river basin in Southern Western Ghats, India. *Environmental Research, Engineering and Management*, 73(4), 41–57. https://doi.org/10.5755/j01.erem.73.4.19553

Welikanna, D., & Jin, S. (2023). Investigating ground deformation due to a series of collapse earthquakes by means of the ps-insar technique and sentinel 1 data in kandy, sri lanka. *Journal of Applied Remote Sensing*, 17(1), 014507. https://doi.org/10.1117/1.jrs.17.014507

Wu, X., Qi, X., Peng, B., & Wang, J. (2024). Optimized Landslide Susceptibility Mapping and Modelling Using the SBAS-InSAR Coupling Model. *Remote Sensing*, 16(16). https://doi.org/10.3390/rs16162873

Yao, Z., Chen, M., Zhan, J., Zhuang, J., Sun, Y., Yu, Q., & Yu, Z. (2023). Refined Landslide Susceptibility Mapping by Integrating the SHAP-CatBoost Model and InSAR Observations: A Case Study of Lishui, Southern China. *Applied Sciences*, 13(23), 12817. https://doi.org/10.3390/app132312817

Yu, W., Li, W., Wu, Z., Lu, H., Xu, Z., Wang, D., Dong, X., & Li, P. (2024). Integrated Remote Sensing Investigation of Suspected Landslides: A Case Study of the Genie Slope on the Tibetan Plateau, China. *Remote Sensing*, 16(13), 2412. https://doi.org/10.3390/rs16132412

Zhang, X., Gan, S., Yuan, X., Zong, H., Wu, X., & Shao, Y. (2024). Early Identification and Characteristics of Potential Landslides in Xiaojiang Basin, Yunnan Province, China Using Interferometric Synthetic Aperture Radar Technology. *Sustainability (Switzerland)*, 16(11), 4649. https://doi.org/10.3390/su16114649